Organic Salts with Large Second-Order Optical Nonlinearities⊥

Seth R. Marder,*,†,‡ Joseph W. Perry,*,†,‡ and Christopher P. Yakymyshyn§

Jet Propulsion Laboratory, California Institute of Technology, 4800 Oak Grove Drive, Pasadena, California, 91109; Molecular Materials Resource Center, The Beckman Institute, California Institute of Technology Pasadena, California, 91125; and Asea Brown Boverie Transmission Technology Institute 1021 Main Campus Drive, Raleigh, North Carolina 27606

Received February 11, 1994. Revised Manuscript Received June 7, 1994®

This paper presents a review of recent work on the development of organic salts for second-order nonlinear optical applications. In particular, salts in which the cation has been designed to have a large molecular hyperpolarizability and in which variation of the counterion facilitates preparation of crystals with the required noncentrosymmetric packing are discussed. In many cases, this approach has led to materials with large powder second harmonic generation (SHG) efficiencies. One salt, *N,N*-dimethylamino-*N'*-methylstilbazolium *p*-toluenesulfonate, DAST, exhibited an SHG efficiency >1000 times that of a urea powder reference. A common layered-polar-sheet crystal packing motif was observed for DAST and several salt crystals that have been examined crystallographically. A possible explanation for the high incidence of noncentrosymmetric packing in these structures is discussed. Finally, the growth and properties of DAST single crystals are reviewed.

Introduction

There is considerable interest in the synthesis of new materials with large second-order optical nonlinearities, because of their potential for use in applications including telecommunications, optical computing, optical data storage, and optical information processing.[1-5] Many such applications require materials with very large macroscopic second-order susceptibilities ($\chi^{(2)}$). Large molecular first hyperpolarizabilities (β) are generally associated with structures that have a large difference between the ground-state and excited-state dipole moments, together with large transition dipole moments and low-energy charge-transfer transitions,[6-8] although new strategies based upon octupolar molecules that have zero dipole moment have recently been explored.[9,10] It is now relatively well understood how to design dipolar organic molecules so as to optimize β.[11,12] However, the molecular nonlinearity associated with a chromophore will lead to a finite $\chi^{(2)}$ for the bulk material only if the chromophores are oriented in a noncentrosymmetric arrangement.[1-5] This requirement is a major impediment when attempting to engineer a material with a large $\chi^{(2)}$. Several approaches have been utilized to artificially achieve noncentrosymmetry, including electric field poling of polymers,[13-16] self assembly of molecular layers[17,18] and Langmuir–Blodgett assembly of films.[19,20] The use of crystalline materials is advantageous for several reasons, including a high number density of chromophore and high thermodynamic orientation stability. On the other hand, crystals generally are not easily processed. An even greater obstacle is that ~75% of all nonchiral organic compounds crystallize in centrosymmetric space groups, in which case the crystal will exhibit no macroscopic second-order optical nonlinearity.[21]

The prediction and/or control of the three-dimensional structure of crystals, given only a knowledge of the

⊥ Dedicated to the memory of Margaret Etter.
† Jet Propulsion Laboratory.
‡ The Beckman Institute.
§ Asea Brown Boverie Transmission Technology Institute.
® Abstract published in *Advance ACS Abstracts,* August 15, 1994.

(1) Prasad, P. N.; Williams, D. J. *Introduction to Nonlinear Optical Effects in Molecules and Polymers*; J. Wiley & Sons, Inc.: New York, 1991, pp 160–174.
(2) Williams, D. J., Ed. *Nonlinear Optical Properties of Organic and Polymeric Materials*; ACS Symposium Series Vol. 233; American Chemical Society: Washington, DC, 1983.
(3) Williams, D. J. *Angew. Chem. Int. Ed. Engl.* **1984**, *23*, 690–703.
(4) Chemla, D. S., Zyss, J., Eds. *Nonlinear Optical Properties of Organic Molecules and Crystals*; Academic Press: San Diego, 1987; Vols. 1, 2.
(5) Marder, S. R., Sohn, J. E., Stucky, G. D., Eds. *Materials for Nonlinear Optics: Chemical Perspectives*; American Chemical Society, Symposium Series Vol. 455; American Chemical Society: Washington, 1991.
(6) Oudar, J. L.; Chemla, D. S. *J. Chem. Phys.* **1977**, *66*, 2664–2668.
(7) Levine, B. F.; Bethea, C. G. *J. Chem. Phys.* **1977**, *66*, 1070.
(8) Lalama, S. J.; Garito, A. F. *Phys. Rev. A* **1979**, *20*, 1179.
(9) Joffre, M.; Yaron, D.; Silbey, R. J.; Zyss, J. *J. Chem. Phys.* **1992**, *97*, 5607–5615.
(10) Zyss, J. *Nonlinear Opt.* **1991**, *1*, 3–18.
(11) Marder, S. R.; Beratan, D. N.; Cheng, L.-T. *Science* **1991**, *252*, 103–106.
(12) Marder, S. R.; Cheng, L.-T.; Tiemann, B. G.; Friedli, A. C.; Blanchard-Desce, M.; Perry, J. W.; Skindhøj, J. *Science* **1994**, *263*, 511–514.
(13) Singer, K. D.; Sohn, J. E.; Lalama, S. J. *Appl. Phys. Lett.* **1986**, *49*, 248–250.
(14) Hubbard, M. A.; Marks, T. J.; Yang, J.; Wong, G. K. *Chem. Mater.* **1989**, *1*, 167–169.
(15) Bjorklund, G. C.; Ducharme, S.; Fleming, W.; Jungbauer, D.; Moerner, W. E.; Swalen, J. D.; Twieg, R. J.; Willson, C. G.; Yoon, D. Y. In *Materials for Nonlinear Optics: Chemical Perspectives;* Marder, S. R.; Sohn, J. E.; Stucky, G. D. Ed.; ACS Symposium Series Vol. 455; American Chemical Society: Washington, DC, 1991; pp 216–225.
(16) Singer, K. D.; Lalama, S. J.; Sohn, J. E.; Small, R. D. In *Nonlinear Optical Properties of Organic Molecules and Crystals;* Chemla, D. S., Zyss, J. Eds.; Academic Press: San Diego, 1987; Vol. 1, p 460.
(17) Li, D.; Ratner, M. A.; Marks, T. J.; Zhang, C.; Yang, J.; Wong, G. K. *J. Am. Chem. Soc.* **1990**, *112*, 7389–7390.
(18) Katz, H. E.; Scheller, G.; Putvinski, T. M.; Schilling, M. L.; Wilson, W. L.; Chidsey, C. E. D. *Science* **1991**, *254*, 1485–1487.
(19) Roberts, G. G. In *Langmuir-Blodgett Films;* Roberts, G. G., Ed.; Plenum Press: New York, 1990; pp 351–368.
(20) Kajikawa, K.; Anzai, T.; Takezoe, H.; Fukuda, A.; Okada, S.; Matsuda, H.; Nakanishi, H.; Abe, T.; Ito, H. *Chem. Phys. Lett.* **1992**, *192*, 113–116.
(21) Nicoud, J. F.; Twieg, R. J. In *Nonlinear Optical Properties of Organic Molecules and Crystals;* Chemla, D. S., Zyss, J., Eds.; Academic Press: San Diego, 1987; Vol. 1, pp 227–296.

0897-4756/94/2806-1137$04.50/0

molecular constituents, is exceedingly difficult and, with our current state of understanding, cannot be done reliably. There have been several studies geared towards rationally designing two dimensional crystal packing motifs. In particular, Etter [22-25] and Lehn[26,27] have focused on designing hydrogen-bonding interactions to encourage specific interactions between molecules and thereby have obtained noncentrosymmetric sheets or chains. Etter et al. have examined a series of nitroaniline materials and found a high occurrence of acentric hydrogen bonded aggregates.[22] Furthermore, they noted that the relatively high occurrence of noncentrosymmetric crystal structures in this class of materials may, in part, be due to the formation of these acentric aggregates. Etter et al. have also shown that *p*-aminobenzoic acid and 3,5-dinitroaniline form a two dimensional acentric sheet in the crystal lattice.[23] In related studies, Lehn has shown that substituted barbituric acids and substituted 1,3,5-triaminopyrimidines can form polar tapes.[27] More recently, Whitesides has also been examining the problem of crystal packing of hydrogen-bonded systems and has demonstrated that relatively complex structures can be assembled by directed hydrogen-bonding interactions.[28] Although researchers have made significant progress in assembling supramolecular structures, we are still far from having the requisite predictive capabilities to allow engineering of three-dimensional crystal structures.

Other groups have approached the problem of crystal packing as a statistical search and have attempted to identify and exploit factors that can enhance the probability of obtaining a noncentrosymmetric packing. Some have attempted to eliminate factors that favor centrosymmetric packing. For example, there have been attempts to reduce the ground-state dipole moment in order to minimize dipole–dipole interactions.[29] Meredith attempted another approach wherein he examined several salts of organic chromophores of the form $(CH_3)_2NC_6H_4CH{=}CHC_5H_4N(CH_3)^+X^-$. He found that the salt with $X = CH_3OSO_3$ had an second harmonic generation (SHG) efficiency roughly 220 times that of urea,[30] which at the time was a record powder SHG efficiency. Moreover, he reported that of the eight salts with different anions that were examined, seven salts exhibited measurable SHG signals, indicative of noncentrosymmetric packing.[30] It was suggested that in salts, Coulombic interactions would overwhelm the deleterious dipole–dipole interactions and, in effect, remove a potential driving force for centrosymmetric crystallization.[30] Some groups have focused on the use of chirality to ensure noncentrosymmetry on the macroscopic level (however, it should be noted that merely appending a chiral group to a chromophore does not ensure a favorable alignment of the chromophores).[21] In particular, amino acid salts[31,32] and saccharides[33-35] have been investigated. While these molecules have small hyperpolarizabilities, they are typically quite transparent, with rather low wavelength cutoffs of less than 300 nm and are therefore of interest for short-wavelength, high-power, frequency conversion applications. With the exception of a few studies, organic salts have been largely ignored for second-order nonlinear optical applications. Building on Meredith's observations, Nakanishi et al.[36-42] and Marder et al.[43-49] have reported that variation of counterions in stilbazolium salts is a simple and highly successful approach to engineering a variety of crystalline materials with very large macroscopic optical nonlinearities. More recently, Zyss et al. have adopted a related approach, termed the organomineralate approach, wherein the anion is typically capable of hydrogen bonding, which has also been relatively successful.[50,51] In this paper, the scope and limitations of the "salt methodology", as applied to stilbazolium systems, are reviewed and common crystal packing motifs that are found in a number of noncentrosymmetric salt systems are discussed. Finally, the initial efforts to assess the utility of highly nonlinear organic salt single crystals for electrooptic device applications are surveyed.

Chromophore Design

Recent experimental[12,52-58] and theoretical[55,59-61] studies of molecular hyperpolarizability have provided guidelines

(22) Panunto, T. W.; Urbánczyk-Lipkowska, Z.; Johnson, R.; Etter, M. C. *J. Am. Chem. Soc.* **1987**, *109*, 7786–7797.
(23) Etter, M. C.; Frankenbach, G. M. *Chem. Mater.* **1989**, *1*, 10–12.
(24) Etter, M. C.; Huang, K. S.; Frankenback, G. M.; Adsmond, D. A. In *Materials for Nonlinear Optics: Chemical Perspectives;* Marder, S. R., Sohn, J. E., Stucky, G. D., Eds.; ACS Symposium Series Vol. 455; American Chemical Society: Washington, DC, 1991; pp 457–471.
(25) Etter, M. C. *J. Phys. Chem.* **1991**, *95*, 4601–4610.
(26) Lehn, J. In *Materials for Nonlinear Optics: Chemical Perspectives;* Marder, S. R., Sohn, J. E., Stucky, G. D., Eds.; ACS Symposium Series Vol. 455; American Chemical Society: Washington, DC, 1991; pp 436–445.
(27) Lehn, J.; Mascal, M.; Cian, A. D.; Fischer, J. *J. Chem. Soc., Chem. Commun.* **1990**, 479.
(28) Seto, C. T.; Whitesides, G. M. *J. Am. Chem. Soc.* **1993**, *115*, 1330–1340.
(29) Zyss, J.; Chemla, D. S.; Nicoud, J. F. *J. Chem. Phys.* **1981**, *74*, 4800.
(30) Meredith, G. R. In *Nonlinear Optical Properties of Organic and Polymeric Materials;* Williams, D. J., Ed.; ACS Symposium Series Vol. 233; American Chemical Society: Washington, DC, 1983; pp 27–56.
(31) Rieckhoff, K. E.; Peticolas, W. L. *Science* **1965**, *147*, 610–611.
(32) Velsko, S. P.; Davis, L.; Wang, F.; Monaco, S.; Eimerl, D. *Proc. SPIE* **1987**, *824*, 178–181.
(33) Halbout, J. M.; Tang, C. L. *IEEE J. Quantum Electron.* **1982**, *18*, 410–415.
(34) Rosker, M. J.; Tang, C. L. *IEEE J. Quantum Electron.* **1984**, *20*, 334–336.
(35) Bourhill, G.; Mansour, K.; Perry, K. J.; Khundkar, L.; Sleva, E. T.; Kern, R.; Perry, J. W.; Williams, I. D.; Kurtz, S. K. *Chem. Mater.* **1993**, *7*, 802–808.
(36) Nakanishi, H.; Kagami, M.; Hamazaki, N.; Watanabe, T.; Sato, H.; Miyata, S. *Proc. SPIE* **1990**, *1147*, 84–89.
(37) Okada, S.; Masaki, A.; Matsuda, H.; Nakanishi, H.; Kato, M.; Muramatsu, R.; Otsuka, M. *Jpn. J. Appl. Phys* **1990**, *29*, 1112.
(38) Okada, S.; Matsuda, H.; Nakanishi, H.; Kato, M.; Muramatsu, R. Japanese Patent 63-348265, 1988.
(39) Koike, T.; Ohmi, T.; Umegaki, S.; Okada, S.; Masaki, A.; Matsuda, H.; Nakanishi, H. *CLEO Technical Digest* **1990**, *7*, 402.
(40) Okada, S.; Masaki, A.; Matsuda, H.; Nakanishi, H.; Kato, M.; Muramatsu, R.; Otsuka, M. *Jpn. Journ. Appl. Phys.* **1990**, *29*, 1112–1115.
(41) Okada, S.; Masaki, A.; Matsuda, H.; Nakanishi, H.; Koike, T.; Ohmi., T.; Yoshikawa, N.; Umegaki, S. *Proc. SPIE* **1990**, *1337*, 178–183.
(42) Sakai, K.; Yoshikawa, N.; Ohmi, T.; Koike, T.; Okada, S.; Masaki, A.; Matsuda, H.; Nakanishi, H. *Proc. SPIE* **1990**, *1337*, 307–313.
(43) Marder, S. R.; Perry, J. W.; Schaefer, W. P. *Science* **1989**, *245*, 626–628.
(44) Marder, S. R.; Perry, J. W.; Tiemann, B. G.; Marsh, R. E.; Schaefer, W. P. *Chem. Mater.* **1990**, *2*, 685–690.
(45) Marder, S. R.; Perry, J. W.; Schaefer, W. P.; Tiemann, B. G.; Groves, P. C.; Perry, K. J. *Proc. SPIE* **1989**, *1147*, 108–115.
(46) Marder, S. R.; Perry, J. W.; Tiemann, B. G.; Schaefer, W. P. *Organometallics* **1991**, *10*, 1896–1901.
(47) Perry, J. W.; Marder, S. R.; Perry, K. J.; Sleva, E. T.; Yakymyshyn, C.; Stewart, K. R.; Boden, E. P. *Proc. SPIE* **1991**, *1560*, 302–309.
(48) Yakymyshyn, C. P.; Marder, S. R.; Stewart, K. R.; Boden, E. P.; Perry, J. W.; Schaefer, W. P. In *Organic Materials for Non-linear Optics II: Royal Society of Chemistry Special Publication No. 91;* Hann, R. A., Bloor, D. Eds.; Royal Society of Chemistry: Burlington House: London, 1991; pp 108–114.
(49) Marder, S. R.; Perry, J. W.; Schaefer, W. P. *J. Mater. Chem.* **1992**, *2*, 985–986.
(50) Kolter, Z.; Hierle, R.; Josse, D.; Zyss, J.; Masse, R. *J. Opt. Soc. Am. B* **1992**, *9*, 534–547.
(51) Zyss, J.; Masse, R.; Bagieu-Beuchler, M.; Levy, J. P. *Adv. Mater.* **1993**, *5*, 120–124.
(52) Singer, K. D.; Sohn, J. E.; King, L. A.; Gordon, H. M.; Katz, H. E.; Dirk, C. W. *J. Opt. Soc. Am. B* **1989**, *6*, 1339–1350.

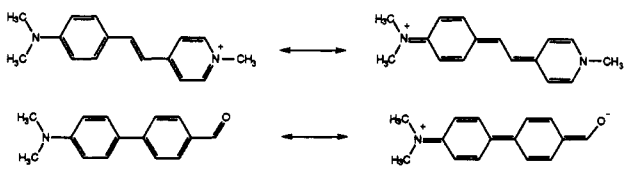

Figure 1. Two limiting canonical resonance forms for (top) a stilbazolium cation and (bottom) and neutral, donor-acceptor biphenyl compound.

Scheme 1

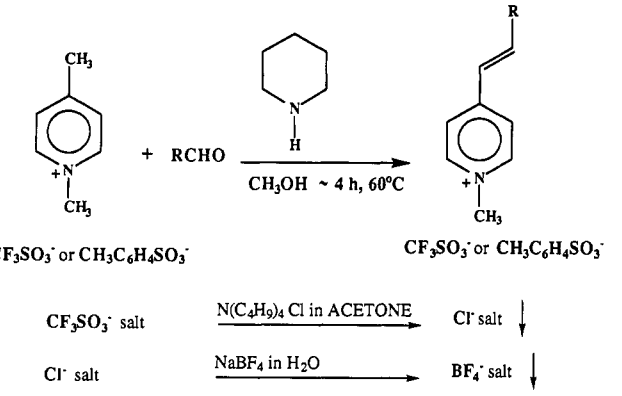

for design of NLO chromophores with large first hyperpolarizabilities, β. The structure of the bridge, as well as nature of the donor and acceptor, plays an important role in determining the value of β. Marder et al. chose to examine cationic chromophores of the general form $RCH{=}CHC_5H_4N(CH_3)^+$, where R is a donor group and the acceptor was either 2- or 4-*N*-methylpyridinium. As is the case with neutral donor-acceptor chromophores, two charge-transfer (CT) resonance forms can be written for stilbazolium cations as shown in Figure 1. Previous studies have suggested that β will be largest when the correct energetic balance between the two CT resonance forms is realized.[55,59] In neutral aromatic molecules of length comparable to that of the stilbazolium cation shown in Figure 1, such as the 4-(*N*,*N*-dimethylamino)-4′-formylbiphenyl (Figure 1), the charge-separated form is higher in energy because charge must be separated and because aromaticity is lost. In the stilbazolium compounds aromaticity is also lost on going from one form to the other but, to a first approximation (i.e., ignoring the interaction with the counterion) charge is not separated in the CT form, it is merely shifted. As a result, the two forms will be closer in energy and likely closer to the optimal energy balance needed to maximize β. Thus, it is expected that the stilbazolium cations will have large β compared to

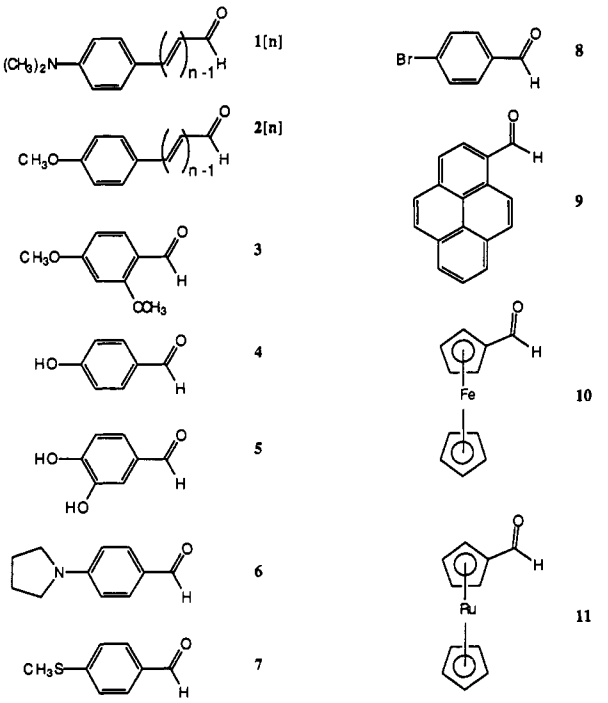

Figure 2. Donor-substituted aldehyde precursors to compounds in Table 1.

neutral aromatic compounds of comparable length. Preliminary estimates of β for stilbazolium chromophores determined by two photon absorption measurements[62] and more recently by hyper-Raleigh scattering (HRS)[63] are in agreement with this hypothesis. For example, Nakanishi et al.[63] have shown by SHG using HRS, that for $CH_3OC_6H_4CH{=}CHC_5H_4N(CH_3)^+X^-$, measured in methanol with 1064 nm fundamental radiation $|\beta|$ is $(360 \pm 80) \times 10^{-30}$ esu, whereas for 4-methoxy-4′-nitrostilbene, $|\beta|$ is 190×10^{-30} esu. Thus, even though the former compound is two atoms shorter than the latter its nonlinearity is significantly larger.[63]

Synthesis and Characterization of Stilbazolium Salts

4-*N*-Methylstilbazolium (or 2-*N*-methylstilbazolium) derivatives are readily synthesized (Scheme 1) by reaction of a 4-*N*-methylpicolinium salt (or a 2-*N*-methylpicolinium salt) and a donor-substituted aldehyde (if the salt has *n* double bonds between the donor and acceptor rings, then the corresponding aldehyde with *n* − 1 C=C double bonds is used, see Figure 2) in methanol, catalyzed by piperidine (or other bases such as pyrrolidine).[64] The reaction is very general and in this manner many 4-*N*-methylstilbazolium derivatives can be prepared. Addition of hydrated tetra-*n*-butylammonium chloride to an acetone solution of 4-*N*-methylstilbazolium trifluoromethanesulfonate gives the corresponding chloride salt (often as an hydrate vide infra) as a fine precipitate. Tetrafluoroborate salts were formed as precipitates when an aqueous sodium tetrafluoroborate solution was added to an aqueous solution of the chloride salts.[44] These salts were then dried and recrystallized from acetone/ether. The labeling scheme for

(53) Cheng, L.-T.; Tam, W.; Stevenson, S. H.; Meredith, G. R.; Rikken, G.; Marder, S. R. *J. Phys. Chem.* **1991**, *95*, 10631–10643.
(54) Cheng, L.-T.; Tam, W.; Marder, S. R.; Steigman, A. E.; Rikken, G.; Spangler, C. W. *J. Phys. Chem.* **1991**, *95*, 10643–10652.
(55) Marder, S. R.; Beratan, D. N.; Cheng, L.-T. *Science* **1991**, *252*, 103–106.
(56) Marder, S. R.; Gorman, C. B.; Tiemann, B. G.; Cheng, L.-T. *J. Am. Chem. Soc.* **1993**, *115*, 3006–3007.
(57) Jen, A. K.-Y.; Rao, P.; Wong, K. Y.; Drost, K. J. *J. Chem. Soc., Chem. Commun.* **1993**, 90–93.
(58) Barzoukas, M.; Blanchard-Desce, M.; Josse, D.; Lehn, J.-M.; Zyss, J. *Chem. Phys.* **1989**, *133*, 323–329.
(59) Gorman, C. B.; Marder, S. R. *Proc. Natl. Acad. Sci. U.S.A.* **1993**, *90*, 11297.
(60) Brédas, J. L.; Dory, M.; Thémans, B.; Delhalle, J.; André, J. M. *Synth. Met.* **1989**, *28*, D533–D542.
(61) Meyers, F.; Adant, C.; Brédas, J. L. *J. Am. Chem. Soc.* **1991**, *113*, 3715–3719.
(62) Birge, R. 1993, personal communication.
(63) Duan, X. M.; Okada, S.; Nakanishi, H.; Clays, K.; Persoons, A.; Matsuda, H. *Proc. SPIE* **1994**, *2143*, 41.
(64) Phillips, A. P. *J. Org. Chem.* **1947**, *12*, 333.

Table 1. Summary of Powder SHG Efficiencies for 4-*N*-Methylstilbazolium Compounds[a]

	counterion			
compound	CF_3SO_3	BF_4	$CH_3C_6H_4SO_3$	Cl
1[1]	0	75[30]	1000	0
	15		15	0
1[2]	500	350	115	0
	5	4	5	0
1[3][49]			6	
2[1]	50	0	115	60
	54	0	101, 30[42]	270
2[2]	0	1	28	48
	0	2	50	4
2[3][49]			5.9	
3	40	6	0	0.4
	67	3	0.1	0.7
4			9[40]	
5[49]			106	
6	0.5	5	0.2	1
	0.1	0.1	0	0
7	0	0		0
	0	0	1	0
8	0	0	2	22
	0	0	5, 1[42]	100
9	1		37	
	1		14	
10[46]	0	50	13	0
11[46]			1	

[a] Values reported are second harmonic intensities relative to that of a urea powder standard. The upper value given is for 1907-nm fundamental radiation, and the lower value is for 1064-nm fundamental radiation. Unless noted otherwise, the values come from ref 43.

aldehyde precursors to stilbazolium salts synthesized by Marder et al. and Nakanishi et al. is shown in Figure 2. The 4-*N*-methylstilbazolium salts are labeled according to the number of the starting aldehyde, appended with the counterion, thus (*N*,*N*-dimethylamino)-*N*′-methylstilbazolium *p*-toluenesulfonate, is **1[1]$CH_3C_6H_4SO_3$**. For **1[1]$CH_3C_6H_4SO_3$**, (also referred to as DAST) the procedure shown in the scheme has been performed on a scale that gave well over 1 kg of product. Several exemplary syntheses are given in the supplementary material. The compounds that were actually examined by Nakanishi et al. and Marder et al. are presented in Table 1.

Characterization of Salts. The salts prepared have been characterized by ^1H nuclear magnetic resonance (NMR) and ultraviolet (UV–vis) spectroscopies, and elemental analysis. In all cases, identification of the cationic chromophore by NMR was routine. The NMR data reported in Table 2 are typically for the trifluoromethanesulfonate salts recorded in $^2H_6$-acetone or ^2H-chloroform because these salts exhibited reasonable solubility in these solvents. In general, the compounds gave almost identical spectra in both solvents and different counterions gave identical cation spectra, indicating that both ions were well solvated. The peaks for the protons on the pyridine rings typically appear downfield of those of the donor-substituted ring, with the protons adjacent to the pyridinium nitrogen characteristically appearing farthest down field, in the range of δ 8.5 –9.0 ppm. The three-bond coupling constant between protons on carbon–carbon double bonds between the donor and pyridinium ring ($^3J_{HH}$) were in the range 15.7–16.5 Hz, indicative of a trans configuration about the double bond (Table 2). Consistent with the large $^3J_{HH}$ was pronounced bond length alternation of the carbon–carbon bonds linking the rings, in the compounds that have been examined crystallographically (Table 2). Thus, the average length of the C–C bonds between the donor or pyridinium ring and the corresponding carbon of the central C=C bond was 1.48 Å and that for the central C=C bonds was 1.30 Å. Information regardingseveral of the crystal structure determinations, not reported in detail elsewhere, is given in Table 3.

In most cases, the elemental analysis was in agreement with a simple cation–anion formulation, however, without exception, the Cl^- salts analyzed low in carbon and nitrogen and high in hydrogen, suggesting that the Cl^- salts may have been isolated as hydrates.[43] This supposition was born out by crystallographic determinations for **2[1] Cl** (vide infra) and **8Cl**, which were identified as tetra hydrates. Such hydrate formation could prove problematical for use of such as nonlinear optical materials, unless steps could be taken to prevent deliquescence. As a result, single-crystal optical studies on chloride salts, even those with large powder SHG efficiencies have not been undertaken (vide infra).

Powder SHG Efficiencies

The SHG efficiencies of various stilbazolium salts synthesized have been characterized[36,37,43–46,49] by the powder technique developed by Kurtz and Perry.[65] A relative measurement of the SHG intensity was made using a reference sample with a known second-order nonlinearity, such as urea. The powder SHG efficiency gave a measure of the product of an average nonlinearity of the crystal (d_{eff}^2) and a factor that depends on the grain size and the coherence length or the phase-matching length, depending on whether the material is phase-matchable. The values reported were typically for samples with a broad distribution of particle sizes (~40–100 μm) thus, the values may influenced by the size dependent factor. Therefore, the reported efficiencies should be taken as a qualitative indicator of crystal nonlinearity, with large values suggesting a potential for large crystal nonlinearities. In any event, a finite SHG signal is a certain indicator of a noncentrosymmetric crystal phase.

As shown in Table 1, many of the stilbazolium salts exhibited SHG. Of particular significance is the observation that for each of the 15 cations in Table 1 a counterion could be found such that the salt had a powder SHG efficiency greater than or equal to that of urea. For the ferrocene compounds it should be noted that the iodide, bromide, and nitrate counterions not listed in Table 1 were the most active with powder SHG efficiencies of 220, 165, and 120 times urea, respectively, measured using 1907-nm fundamental radiation.[46] For the 43 salts in Table 1, 32 had SHG efficiencies greater than or equal to 0.1 times that of urea. In contrast, for the 11 2-*N*-methylstilbazolium salts (seven different cations) that were examined only three exhibited SHG.[44] These observations suggest that the asymmetric structure of the 2-*N*-methylstilbazolium cations compared to the more rodlike 4-*N*-methylstilbazolium salts interferes with interactions favoring noncentrosymmetric packing in the latter compounds, thereby tending to favor centrosymmetric packing.[44] This is in contrast to neutral dipolar chromophores, such as nitroa-

(65) Kurtz, S. K.; Perry, T. T. *J. Appl. Phys.* **1968**, *39*, 3798.

Table 2. Summary of ^1H NMR Coupling Constant Data and Crystallographically Determined Bond Lengths for the Ethylenic Bridge of Selected Compounds in Table 1

compound	$^3J_{HH}$(C=C)	donor ring (C)—C=	ethylenic C=C	=C—pyridinium ring (C)	ref
1[1]$CH_3C_6H_4SO_3$	16.1	1.451(3)	1.337(4)	1.449(4)	43, 68
2[1]$CH_3C_6H_4SO_3$	16.5	1.463(5)	1.325(5)	1.462(5)	43, 68
2[1]$Cl(H_2O)_4$		1.498(6)	1.304(7)	1.463(6)	43, 68
3CF_3SO_3	16.6	1.455(7)	1.258(8)	1.515(8)	68
4$CH_3C_6H_4SO_3$	16.3	1.454(4)	1.300(5)	1.482(4)	37
5$CH_3C_6H_4SO_3$		1.457(3)	1.339(3)	1.451(3)	49
6CF_3SO_3	16.0				43, 68
7CF_3SO_3	16.2				43, 68
8$Cl(H_2O)_4$	16.5	1.449(16)	1.315(15)	1.486(14)	43, 68
9CF_3SO_3	16.1				43, 68
10NO_2	15.7 (I^- salt)	1.493(16)	1.234(17)	1.580(16)	46
11CF_3SO_3	16.0				46

Table 3. Summary of Crystallographic Data for 1[1]$CH_3C_6H_4SO_3$, 2[1]$CH_3C_6H_4SO_3$, 2[1]$Cl(H_2O)_4$, 5$CH_3C_6H_4SO_3$, and 8$Cl(H_2O)_4$

	1[1]$CH_3C_6H_4SO_3$	2[1]$CH_3C_6H_4SO_3$	2[1]$Cl\cdot 4H_2O$	5$CH_3C_6H_4SO_3$	8[1]$Cl\cdot 4H_2O$
reference	43	68	68	49	68
formula	$C_{23}H_{26}N_2SO_3$	$C_{22}H_{23}NSO_4$	$C_{15}H_{16}NO$ $Cl\cdot 4H_2O$	$C_{21}H_{22}NSO_5$	$C_{14}H_{13}NBr$ $Cl\cdot 4H_2O$
formula weight	410.54	397.50	333.82	400.48	382.69
crystal system	monoclinic	monoclinic	orthorhombic	triclinic	orthorhombic
space group	*Cc*, No. 9	$P2_1$, No. 4	$Pna2_1$, No. 33	*P*1, No. 1	$Pna2_1$, No. 33
cell dimensions					
a, Å	10.365(3)	9.567(1)	18.138(4)	6.591(2)	17.631(6)
b, Å	11.322(4)	6.511(1)	7.030(1)	8.175(2)	7.070(7)
c, Å	17.893(4)	15.902(2)	13.982(5)	9.128(2)	13.946(6)
α, deg	90	90	90	102.45(2)	90
β, deg	92.24(2)	91.78(1)	90	94.02(3)	90
γ, deg	90	90	90	96.62(3)	90
V, Å^3	2098.2(11)	990.1(2)	1782.8(8)	474.8(2)	1738(2)
Z	4	2	4	1	4
density, calc, g cm^{-3}	1.300	1.33	1.24	1.40	1.45
crystal shape	chunky prism	irregular cut chunk	irregular cut chunk	triangular pyramid	nearly cubic chunk
crystal size, mm	0.11 × 0.14 × 0.17	0.37 × 0.33 × 0.54	0.41 × 0.60 × 0.52	0.20 × 0.23 × 0.70	0.13 × 0.29 × 0.24
μ, cm^{-1}	1.72	1.93	2.40	2.06	26.47[c]
μr_{max}	0.05	0.07	0.11	0.08	0.65
max 2θ (scan type)	40° (ω)	50° (θ–2θ)	40° (ω)	60° (θ–2θ)	40° (θ–2θ)
range of *h*,*k*,*l*	±12, ±13, 0–21	±11, ±7, 0–18	0–19, ±7, ±14	±9, ±11, ±12	0–17, ±7, ± 13
no. of reflns measured	3891	4748	4914	5647	3770
no. of independent reflns	1850	1909	1218	2771	1635
no. of reflns, $\|F^2_o\|>0$	1777	1815	1170	2744	1515
no. of reflns, $F_o^2 > 3\sigma(F_o^2)$	1580	1789	1012	2618	1228
GOF, merge	0.99	1.28	1.11	1.13	1.55
R (merge) for refs measd twice				0.015	
secondary extinction					0.26(7) × 10^{-6}
$R, F_o^2 > 0$	0.033	0.044	0.040	0.032	0.049
$R, F_o^2 > 3\sigma(F_o^2)$	0.028	0.043	0.034	0.030	0.036
GOF (number of parameters)	1.81 (262)	4.03 (322)[a]	2.85 (198)[b]	2.24 (250)	1.87 (222)[b]
$(\Delta/\sigma)_{max}$ in least squares	0.02	0.04	0.01	<0.01	0.06(0.11 for H)
final difference map					
max, e Å^{-3}	+0.25	+0.30	+0.15	+0.18	+1.19 - near Br
min, e Å^3	−0.25	−0.32	−0.14	−0.19	−1.12 - near Br

[a] Hydrogen atom parameters were refined. [b] Some hydrogen parameters were refined. [c] Analytical absorption correction applied; transmission factors 0.46–0.55.

nilines, where introduction of molecular asymmetry increases the probability of noncentrosymmetric packing.[66]

p-Toluenesulfonate salts of 4-*N*-methylstilbazolium cations exhibit a particularly high incidence of noncentrosymmetric packing. Marder et al. synthesized 14-donor-substituted 4-*N*-methylstilbazolium *p*-toluenesulfonate salts[43,46,49] and Okada et al. independently studied 1[1]-**$CH_3C_6H_4SO_3$**, 2[1]**$CH_3C_6H_4SO_3$**, as well as 4 **$CH_3C_6H_4SO_3$**[37,40–42] (see Table 1), and one acceptor-substituted 4-cyano- 4′-*N*-methylstilbazolium cation, as the $CH_3C_6H_4SO_3^-$ salt (where the SHG efficiency was 3.8 times that of urea measured with 1064-nm fundamental radiation).[42] Of the 16 donor-substituted and one acceptor substituted 4-*N*-methylstilbazolium *p*-toluenesulfonate salts described here, 12 had powder SHG efficiencies greater than urea. The approximately 75% incidence of noncentrosymmetric crystallization observed for these salts compares favorably to the roughly 25% incidence of noncentrosymmetric crystallization[21] in nonchiral organic materials studied crystallographically. Of particular interest was compound 1[1]**$CH_3C_6H_4SO_3$** (DAST), that had a powder SHG efficiency (with 1907-nm fundamental radiation) > 1000 times that of a urea reference.[43] Accordingly, single crystals of this salt have been grown and studied in some detail (vide infra).

(66) Tweig, R. J.; Jain, K. In *Nonlinear Optical Properties of Organic and Polymeric Materials;* Williams, D. J., Ed.; ACS Symposium Series Vol. 233; American Chemical Society: Washington, DC, 1983; pp 57–80.

(67) Tam, W.; Wang, Y.; Calabrese, J. C.; Clement, R. A. *Proc. SPIE* 1988, *971*, 107–112.

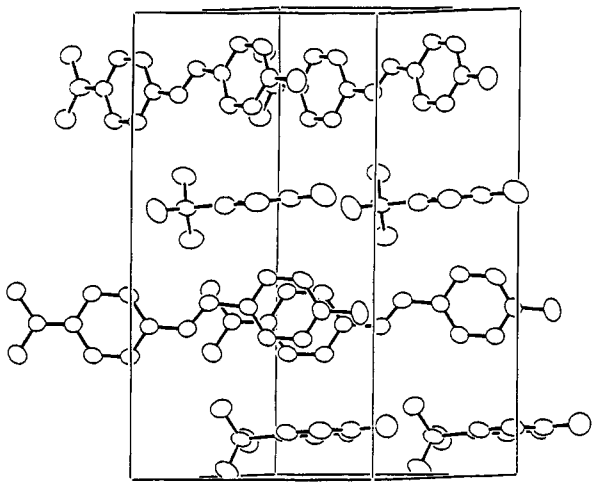

Figure 3. Packing drawing of DAST, showing the contents of a unit cell (hydrogen atoms are not shown) viewed roughly perpendicular to the *c* axis.

An Example of Hydration Leading to Noncentrosymmetry

Some neutral organic compounds are known to crystallize in various crystal phases as a function of crystallization conditions. Tam has demonstrated that this phenomena can be used to manipulate the packing of relatively nonpolar stilbenes.[67] Both Nakanishi et al. and Perry et al.[47] have observed that different solvents and growth conditions could lead to different phases for organic salts. Furthermore, it was observed in several cases that compounds can be isolated with varying numbers of water molecules in the crystallographic lattice. One of the more intriguing cases is that of the **2[1]Cl**, which can be isolated as a yellow hydrated phase which has been crystallographically characterized and is SHG active.[68] When powders of this compound are either subjected to vacuum or left open in a dry environment (i.e., in open air in Pasadena California) for months, the sample turns orange and becomes SHG inactive upon excitation at 1064 nm.[68] However, a red emission, likely due to fluorescence following two-photon absorption, is seen. If a sample of the SHG inactive material was exposed to water (vapor or a small drop of liquid), without apparent dissolution of the sample, the material again became yellow in color and SHG active. This procedure could be repeated at least several times.[68] The hydrate has been shown to be noncentrosymmetric crystallographically, consistent with the large SHG activity. The transition to an SHG inactive phase upon dehydration indicates conversion to a centrosymmetric structure. It is interesting that such a structural reorganization can occur totally in the solid state. However, although such processes would likely limit the utility of this salt as a single-crystal nonlinear optical material, it could conceivably be utilized as a remote sensor for humidity.

Crystal Packing

A general structural motif common to seven of the compounds that have been structurally characterized has been observed and is illustrated in Figures 3–6 for compounds DAST, **$5CH_3C_6H_4SO_3$**, **$2[1]Cl(H_2O)_4$**, and **$8Cl(H_2O)_4$**. It was also observed in P1 phases of **$2[1]$-$CH_3C_6H_4SO_3$**[42] and **$4CH_3C_6H_4SO_3$**[40] by Nakanishi et al. and in a 3′-methoxy-2-*N*-methylstilbazolium trifluoromethanesulfonate Marder et al. had examined earlier.[44] The tendency for flat aromatic molecules to stack, coupled with the electrostatic attraction between the donor of one molecule and the acceptor of an adjacent molecule, appears to favor formation of polar sheets of cations. For example, in DAST, the sheets of cationic chromophores are interleaved with sheets of *p*-toluenesulfonate anions. The planes of the *p*-toluenesulfonate rings lie in the plane of

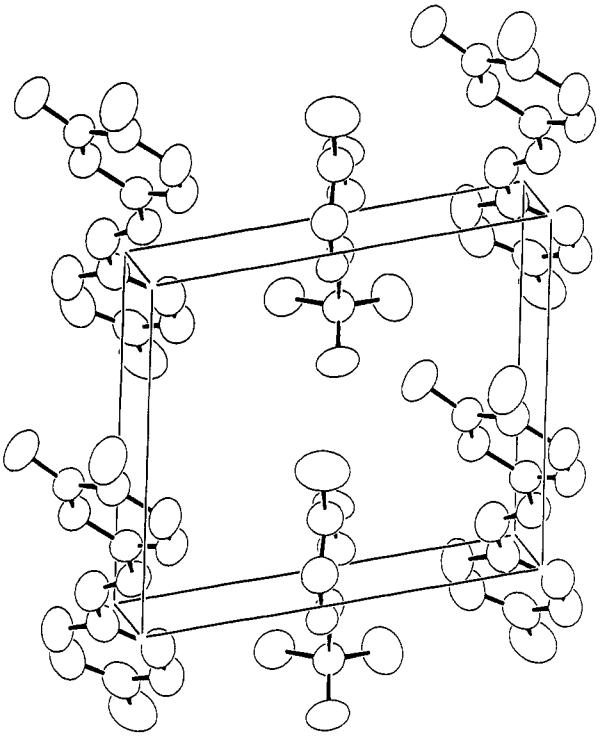

Figure 4. Packing drawing of **$5CH_3C_6H_4SO_3$**, showing four cations and two anions, with a unit cell outlined (hydrogen atoms are not shown), viewed perpendicular to the *bc* plane.

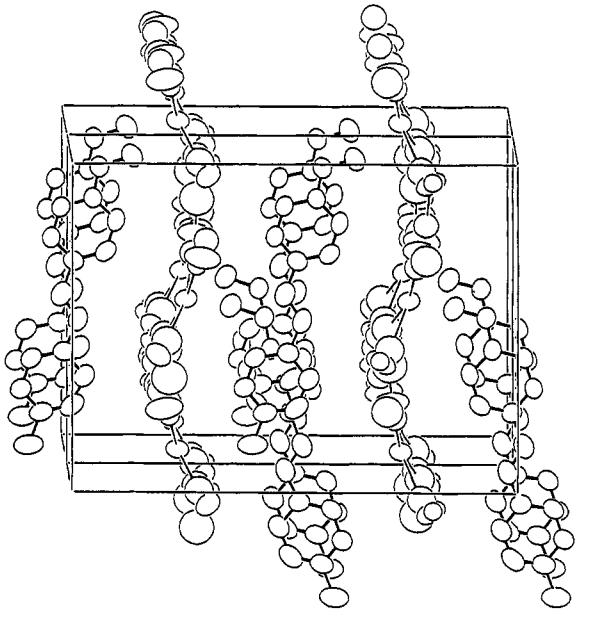

Figure 5. Packing drawing of **$2[1]Cl(H_2O)_4$**, showing two unit cells outlined, with eight cations and many constituents of the chloride–water network. Hydrogen atoms are shown only on water molecules, and hydrogen bonds are indicated by thin lines.

(68) Marder, S. R.; Perry, J. W.; Schaefer, W. P., 1994, unpublished results.

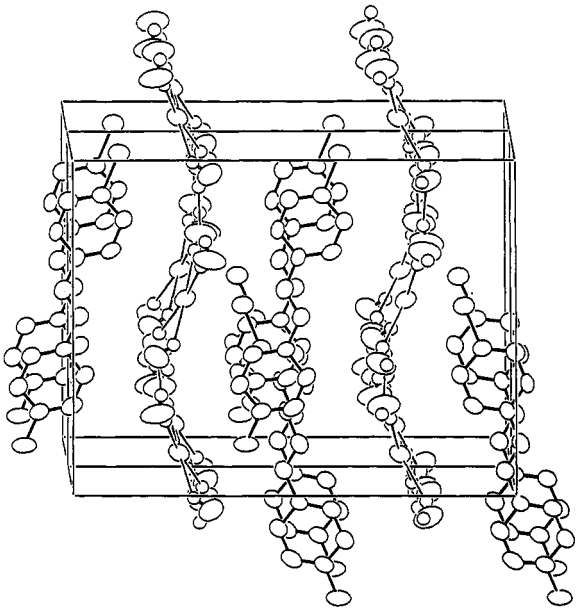

Figure 6. Packing drawing of $8Cl(H_2O)_4$, showing two unit cells outlined, with eight cations and many constituents of the chloride–water network. Hydrogen atoms are shown only on water molecules, and hydrogen bonds are indicated by thin lines.

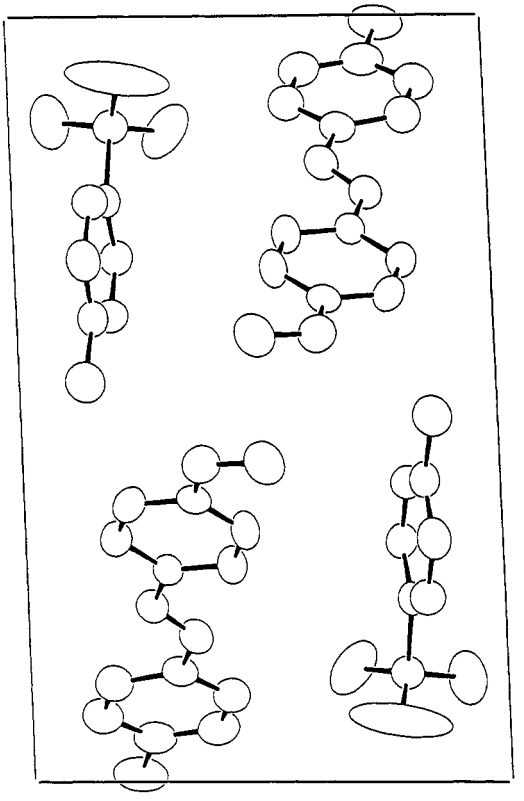

Figure 7. Packing drawing of $2[1]CH_3C_6H_4SO_3$, showing the contents of a unit cell (hydrogen atoms are not shown) viewed down the *b* axis.

the anion sheet and are roughly perpendicular to the molecular planes of the cations. A single crystal structure determination was performed on $2[1]CH_3C_6H_4SO_3$, crystallized by either vapor-phase diffusion of diethyl ether into a nearly saturated solution of methanol or by slow cooling of a warm methanol solution. Interestingly, in contrast to the P1 phase obtained by Nakanishi et al., by slow evaporation of a methanol solution,[42] Marder et al. isolated a $P2_1$ phase by slow cooling, for which a packing

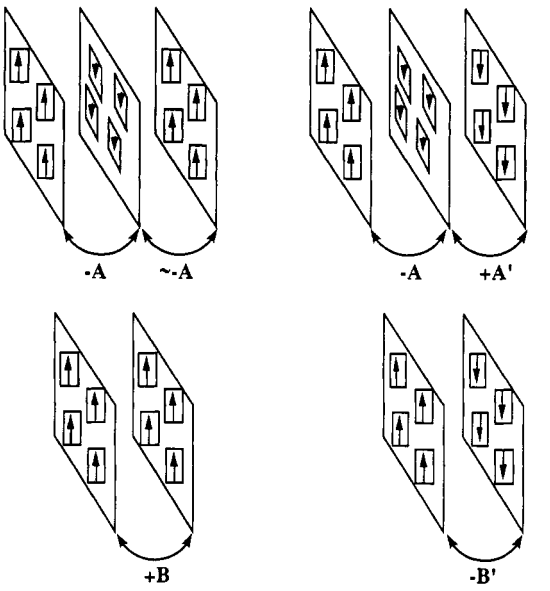

Figure 8. (Upper left) parallel alignment of polar sheets for a salt; (upper right) antiparallel alignment of polar sheets for a salt; (lower left) parallel alignment of polar sheets for a neutral dipolar compound; (lower right) parallel alignment of polar sheets for a neutral dipolar compound. The letters A, A′, B, and B′ generically label an overall interaction energy between the adjacent sheets; the minus and plus signs indicate whether this interaction is net stabilizing or destabilizing, respectively.

diagram is shown in Figure 7.[68] Apparently, very subtle differences in growth conditions can lead to different phases that, as can be seen in Table 1, also have significantly different powder SHG efficiencies.

Both Nakanishi[40] and Marder et al.[49] have suggested that the formation of alternating cationic and anionic sheets can facilitate the formation of macroscopically polar structures. Marder et al. proposed that donor–acceptor, hydrogen-bonding, and π–π stacking interactions often yield polar sheet structures. In neutral dipolar molecules steric and/or Coulombic interactions (indicated by -B′, Figure 8, lower right) between neighboring sheets, often lead to an antiparallel orientation of adjacent sheets (Figure 8, lower right).[49] In several of the noncentrosymmetric salts that have been structurally characterized, polar cationic sheets are separated by sheets of anions (see Figures 3–6). As a result, the interactions between the cationic sheets, in effect, may be mediated by interactions with the intervening anion sheet. A combination of steric and Coulombic interactions (indicated by +A, Figure 8, upper left) will define the most favorable orientation of the anion sheet (which may be polar) with respect to the cationic sheet.[49] Since the anion sheets are roughly planar or have approximate mirror symmetry, with respect to the plane of the anion, similar interactions to those that dictated the preferred orientation between the anion sheet and the first cation sheet could provide a driving force to align a subsequent cation sheet roughly parallel to the first. Thus, the anion sheet could provide a driving force *favoring* a net polar alignment of cation sheets (Figure 8, upper left) and *disfavoring antiparallel alignment* (Figure 8, upper right).[49] However, since there is not exact mirror symmetry in the lattice for compounds shown in Figures 3–6, the above explanation is approximate. Nonetheless, it was suggested that the symmetry or pseudosymmetry of interactions in two component polar, layered lattices could give rise to a higher incidence of *polar three*

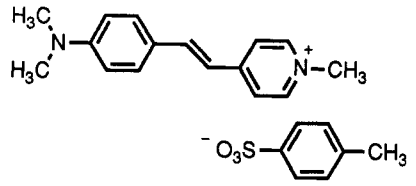

Figure 9. Molecular structure of DAST.

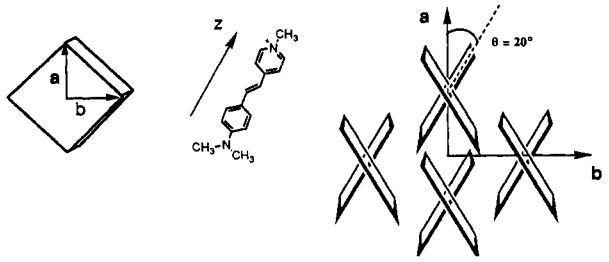

Figure 10. Schematic illustration of (left) DAST crystal habit showing orientation of crystal axes relative to habit geometry; (center) z axis definition for β tensor and (right) orientation of chromophores relative to crystal axes.

dimensional packing arrangements, than for single component systems, despite the fact that all of the interactions are not necessarily controlled.[49]

Studies of DAST Single Crystals

The large powder SHG efficiencies and the nearly fully aligned chromophore orientations in the crystals observed for many of the stilbazolium salts examined suggested that these crystals should exhibit large nonlinear optical and electrooptic coefficients. Of the various stilbazolium salts examined to date DAST, whose molecular structure is shown in Figure 9, exhibited the highest powder SHG efficiency at about 1000 times that of urea.[43] As a result single crystals of DAST were grown to allow optical characterization.

Crystal Growth. Single crystals of the monoclinic Cc phase of DAST were grown either by temperature lowering of saturated methanol solutions, slow evaporation of methanol solutions, or by diffusion of diethyl ether, a nonsolvent for DAST, into a saturated methanol solution.[47,48] Specimens of variable quality with well formed habits of dimensions up to about 5 × 5 × 1 mm^3 were obtained from evaporation and cooling. Ether diffusion produced smaller but nearly defect free crystals up to 2 × 2 × 0.1 mm^3, with highly reflective facets. Single crystals of the Cc phase of DAST exhibit a green reflective luster and appear red in transmission. It should be noted that an SHG inactive phase of hydrated DAST (orange in color) can be obtained, but with suitable attention to exclusion of moisture from the growth solution, the highly SHG active Cc phase can be obtained reliably.

Thermal, Structural and Optical Properties. Thermal studies indicate that DAST is a thermally stable organic crystal. Differential scanning calorimetry shows a clean melting endotherm at 256 °C and no crystal–crystal phase transitions at lower temperatures. Thermogravimetric analysis shows no weight loss until above 290 °C. Furthermore, crystals of DAST displayed no apparent change in optical properties after being heated to 160 °C for 200 h in air.[69]

(69) Yakymyshyn, C. P., 1994, unpublished results.

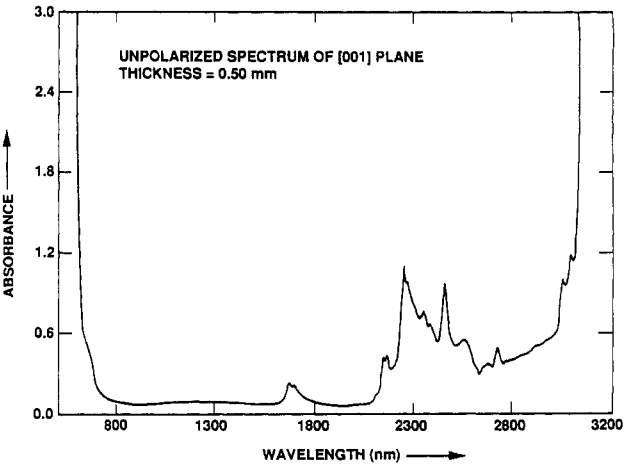

Figure 11. Visible near–IR absorption spectrum of DAST single crystal.

X-ray studies of DAST single crystals revealed that the large face of the plates contains the ab plane of the crystal structure with the a and b axes along the diagonals. The herringbone chromophore orientation in the ab plane is such that the long axis of the chromophores makes an angle of about 20° with respect to the a axis of the crystal (Figure 10).[47,48] The chromophore sheets are stacked along the [001] direction which is nearly along c, since the monoclinic angle β in DAST is 92.2°.

Figure 11 shows the unpolarized visible/near-IR absorption spectrum of the [001] plane of a DAST crystal.[47] Below about 700 nm there is strong absorption correlating to the solution charge transfer absorption band (λ_{max} = 474 nm, ϵ = 40 000 L mol^{-1} cm^{-1} in methanol). The crystal is quite transparent at longer wavelengths down to about 2100 nm, with weak absorption bands at about 1700 nm. The crystal becomes very strongly absorbing above 3000 nm. These near-IR absorptions are due to CH overtone and combination bands. In the technologically important range from 750 nm to about 1650 nm, the absorption is very weak. Recent measurements by Knopfle et al., show that the loss coefficients at the wavelengths of minimum absorption, i.e., near 1550 nm, are <4 cm^{-1}, with this loss likely being due mainly to scattering in the crystal.[70] The absorption edge of the crystal near 700 nm shows a strong dichroism with stronger absorption for light polarized along a, consistent with the chromophore orientation.

The refractive indices of DAST crystals were initially measured by the Brewster angle method[48] and have more recently been determined more accurately, over the range from 770–1907 nm, using an interferometric method.[70] The b crystal axis, which is perpendicular to a mirror plane, is required by symmetry to be a principal dielectric axis, the Y axis, of the crystal, but the X and Z axes are not constrained in the perpendicular plane, by symmetry. Nonetheless, because of the dominant role of the chromophores in determining the optical properties and the small angle they make with the a axis, the X dielectric axis nearly coincides with a. Since, the monoclinic angle β is close to 90°, the Z axis is likewise close to c. DAST is a positive biaxial crystal, with the X axis possessing the largest refractive index. DAST crystals show large birefringence with n_1 = 2.2 at 820 nm, being much larger than n_2 = 1.67 and n_3 = 1.65, (Knöpfle et al.[70] determined n_1

(70) Knöpfle, G.; Schlesser, R.; Ducret, R.; Günter, P. *Nonlinear Opt.*, in press.

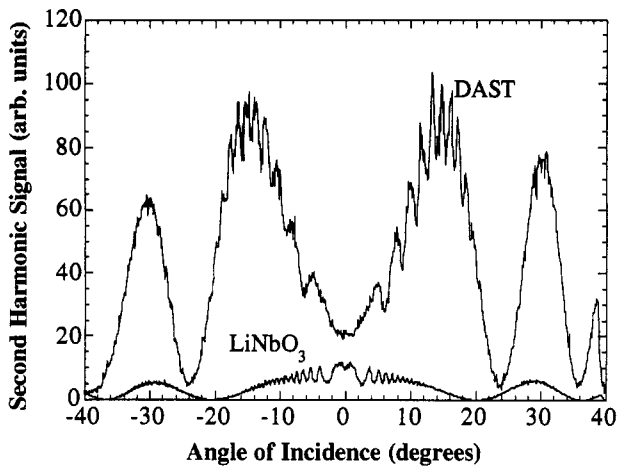

Figure 12. SHG maker fringes for (top) DAST and (bottom) $LiNbO_3$ crystals. Measurements with 1907-nm fundamental.

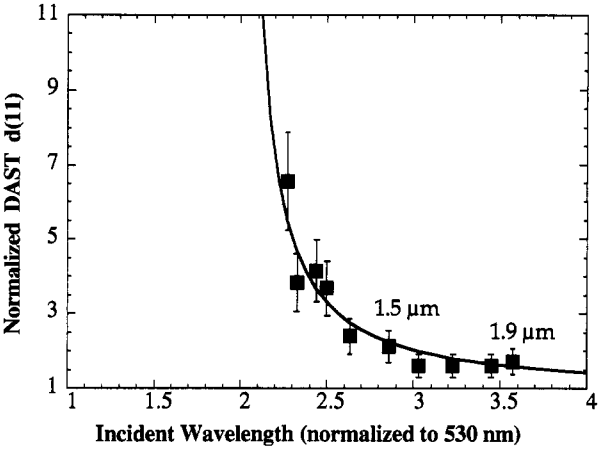

Figure 13. Dispersion of d_{11} for DAST crystals in the near-IR region.

= 2.46, n_2 = 1.68, and n_3 = 1.61 at 805 nm) consistent with the chromophore orientation. The large refractive indices are advantageous for electrooptic applications, since an electrooptic material figure-of-merit is given by FOM = n^3r. The dielectric constants of DAST have been determined, in the 1–100 kHz range, to be $\epsilon_a = 7.0$, $\epsilon_b \approx \epsilon_c = 3.1$, which are close to the far off-resonance values of n^2, suggesting minimal orientational or vibrational contribution to the dielectric response of the crystal, over this range of frequencies.[48]

Single Crystal Nonlinear Optical Properties. As mentioned above, given the orientation of the chromophores in the crystal, large nonlinear optical coefficients are expected for DAST single crystals. On the molecular level, one expects that the only significant component of the hyperpolarizability tensor β for the chromophore, is along the charge-transfer axis of the molecule, i.e., β_{zzz}. Using the orientation of the chromophores in the crystal, one can, in the context of an oriented gas description, estimate the projection of the hyperpolarizability along the a axis using $\beta_{aaa} = \beta_{zzz} \cos^3\theta$, from which one finds $\beta_{aaa} = 0.83\ \beta_{zzz}$. The crystal nonlinear optical coefficient d_{11} and the electrooptic coefficient r_{11} would both be proportional to this projection and can be seen to express a large fraction of the chromophore hyperpolarizability. One can also estimate d_{12} or r_{12} which are proportional to $\beta_{abb} = \beta_{zzz} \cos\theta \sin^2\theta = 0.11\beta_{zzz}$. Thus, the oriented gas model, assuming only a β_{zzz} component for the stilbazolium chromophore, leads to a prediction of d_{11}/d_{12} or r_{11}/r_{12} = 7.5. This value should be viewed as a crude estimate since it neglects any difference in local fields, contributions from projections of other hyperpolarizability tensor components, or contributions from the anions.

The nonlinear susceptibility of DAST was measured using the conventional Maker Fringe method. Preliminary results on DAST crystals at 1907 nm have been reported by Perry et al.[47] and gave d_{11} = 600 ± 200 pm/V at 1907 nm and a coherence length of L_{coh} = 2.6 μm. The measurements were made using a lithium niobate reference sample (d_{33} = 30 pm/V).[71] Figure 12 shows the Maker fringes from a more recent the d_{11} determination[72] at 1907 nm, which give d_{11} and L_{coh} consistant with the earlier values. Measurements on a number of independent crystal specimens indicate substantial crystal-to-crystal variations in the magnitude of the nonlinearity, which is attributed to variations in crystal quality. Measurements were performed under different polarization conditions to allow the determination of d_{11} and d_{12}, and these results are summarized in Table 4.[47] The DAST d coefficients have recently been determined by Knöpfle et al.,[70] and these measurements gave somewhat lower values for the nonlinear coefficients (e.g., d_{11} = 330 ± 80 pm/V and d_{12} = 20 ± 5 pm/V at 1907 nm), but nonetheless confirm that DAST exhibits large nonlinear optical coefficients. Both sets of measurements gave a large d_{11}/d_{12} ratio, with values of ~15–20. This value of the ratio is even larger than that predicted above, using the oriented gas model, but is qualitatively consistent with the crystal nonlinearity being dominated by the projection of the stilbazolium chromophore's β_{zzz}. The dispersion of d_{11} in DAST was measured from 1200–1907 nm, using a potassium titanylphosphate (KTP) optical parametric oscillator, and the d_{11} values are shown in Figure 13.[72] When a two-level model for the dispersion of the d coefficient is superimposed on the collected data, excellent agreement with the data was observed. Nakanishi et al. have also performed single crystal SHG studieds on **2[1]$CH_3C_6H_4SO_3$**[73] and **4$CH_3C_6H_4SO_3$**[40] and has found that these salts also have exceptionally large d coefficients, measured using 1064-nm fundamental radiation. Thus, **2[1]$CH_3C_6H_4SO_3$**[73] and **4$CH_3C_6H_4SO_3$**[40] gave d_{11} = 190 pm/V and 500 ± 63 pm/V, respectively.

Electrooptic Coefficient of DAST Crystals. Yakymyshyn et al. reported preliminary measurements of the electrooptic coefficients of DAST.[48] The electrooptic coefficient measurements used the method previously described by Yoshimura.[74] From the determined electric-field-induced phase delay, an electrooptic figure-of-merit is calculated using FOM = $n_1^3 r_{11} - n_2 r_{12}^3 = \lambda\Gamma_m D/(\pi V_m L)$ where Γ_m is the electrooptically induced phase delay, D is the electrode spacing, V_m is the applied voltage, and L is the effective crystal thickness. These initial measure-

(71) Singh, S. In *Handbook of Lasers;* Pressley, R. J., Ed.; CRC Press: Cleveland, 1971; p 514.

(72) Lawrence, B. Masters Thesis, Massachusetts Institute of Technology, 1992.

(73) Okada, S.; Masaki, A.; Sakai, K.; Ahmi, T.; Koike, T.; Anzai, E.; Umegaki, S.; Matsuda., H.; Nakanishi, H. In *Nonlinear Optics: Fundamentals, Materials and Devices;* Miyata, S., Ed.; Elsevier Science Publishers: North-Holland, 1992; pp 237–242.

(74) Yoshimura, T. *J. Appl. Phys.* **1987**, *62*, 2028.

Table 4. Summary of DAST Crystal Properties

crystal structure	monoclinic Cc, acentric, $Z = 4$
melting point	256–260 °C
axis convention	$b \parallel 2 \parallel Y$; $c \parallel 3 \parallel Z$; $a = b \times c$
absorption peak (λ_{max})	
solution	474 nm
single crystal	540 nm along a axis
indices of refraction	
	$n_1^2 = 4.43 + 0.17/(\lambda^2 - 0.32)$
	$n_2^2 = 2.59 + 0.082/(\lambda^2 - 0.26)$
	$n_3^2 = 2.60 + 0.51/(\lambda^2 - 0.22)$
pockels coefficient	$r_{11} = 160 \pm 50$ pm/V @ 820 nm
NLO coefficients	$d_{11} = 475 \pm 150$ pm/V @ $\lambda = 1907$ nm[47,72]
	$= 330 \pm 80$ pm/V @ $\lambda = 1907$nm[70]
	$= 600 \pm 200$ pm/V @ $\lambda = 1600$ nm[72]
	$= 540 \pm 110$ pm/V @ $\lambda = 1542$ nm[70]
	$= 1050 \pm 250$ pm/V @ $\lambda = 1300$ nm[72]
	$= 1900 \pm 500$ pm/V @ $\lambda = 1200$ nm[72]
	$d_{12} = 200 \pm 50$ pm/V @ $\lambda = 1907$ nm[72]
	$= 30 \pm 10$ pm/V @ $\lambda = 1907$ nm[47]
	$= 21 \pm 5$ pm/V @ $\lambda = 1907$ nm[70]
	$d_{26} = 30 \pm 10$pm/V @ $\lambda = 1907$ nm[72]
	$= 20 \pm 4$ pm/V @ $\lambda = 1907$ nm[70]
dielectric constants	ϵ_a = 7.0 @ 1–100 kHz
	= 8.0 @ 2–20 GHz[80]
	= 7 @ 200–2000 GHz[80]
	$\epsilon_b \approx \epsilon_c$ = 3.1 @ 1–100 kHz
	= 2.9 @ 2–20 GHz[80]
	= 4 @ 200–2000 GHz[80]

Table 5. Comparison of Optical and Electrooptic Properties of Several Inorganic and Organic Crystals

material	ref	measurement wavelength (nm)	n	r (pm/V)	n^3r (pm/V)
$LiNbO_3$	75	632.8	2.2	31	330
GaAs	75	900	3.5	1.5	64
MNA[a]	76	632.8	2.0	67	536
MNBA[b]	77	610	2.04	30	255
DAST	48	820	2.2	160	1700

[a] MNA: 2-methyl-4-nitroaniline. [b] MNBA: 4-methoxy-3-acetamido(4'-nitrobenzylidenyl)aniline.

ments gave FOM = 4200 pm/V, or, assuming $n_1^3 r_{11} \gg n_2^3 r_{12}$, $r_{11} = 400$ pm/V (taking $n = 2.2$).[47] However more recent measurements on several crystals give FOM = 1700 pm/V or $r_{11} = 160 \pm 50$ pm/V at 820 nm and are consistent with an r_{11} coefficient calculated using a two-state model and the reported d_{11} coefficients.[69]

The electrooptic coefficient of DAST is compared with those of other inorganic and organic crystals in Table 5.[75–77] A more detailed comparison of organic electrooptic crystals has been presented by Bosshard et al.[78] As can be seen in Table 5 the electrooptic properties of DAST compare favorably with the other materials and it exhibits a large n^3r. Thus, electrooptic modulators based on DAST crystals offer the potential devices with low drive voltages. Furthermore, due to relatively low dielectric constant, the figure of merit for power consumption of DAST ($n^3r/\epsilon = 240$ pm/V) is 20 times higher than that of $LiNbO_3$ ($n^3r/\epsilon = 12$).[75] However, since the electrooptic coefficient measured at 820 nm is relatively close to the wavelength of the electronic absorption, significant dispersion is expected. Thus at the technologically important wavelengths of 1300 and 1550 nm, the electrooptic coefficient will be smaller. Accordingly, it will be of considerable interest to measure the dispersion of the electrooptic coefficient of DAST in the near infrared region.

Studies of the electrooptic properties of DAST at high frequencies and of terahertz generation in DAST have appeared. The dispersion of the electrooptic coefficient r_{11} of DAST has been measured between 1 and 40 GHz.[79] The microwave measurements were performed using a coplanar transmission line to couple a traveling electromagnetic wave into a DAST crystal pressed against the transmission line. A synchronized optical pulse probed the induced optical birefringence, and sequential sampling allowed reconstruction of the electrooptic response. The electrooptic response was flat from 1–40 GHz, and the material showed no signs of photobleaching during the course of the experiments at 1064 nm. Terahertz (THz) optical rectification in a DAST crystal has been reported.[80] A femtosecond near infrared pulse was focused into a DAST single crystal and the resulting terahertz propagating beam was detected using a conventional terahertz pump-probe arrangement. The detected terahertz signal amplitude was 200 times larger than that generated by lithium tantalate and 42 times larger than that generated by an unbiased GaAs sample.

Conclusions

We have reviewed the preparation and properties of a series of 4-*N*-methylstilbazolium salts that display very large second-order nonlinear susceptibilities. Powder SHG measurements demonstrated a >85% success rate in isolating acentric *p*-toluenesulfonate salts. Crystal structures of six salts have the common feature of parallel-aligned nonlinear chromophore sheets separated by sheets of "spacer" counterions. Single crystals of the highly nonlinear material, DAST, have been grown, and preliminary measurements of the optical, dielectric and electrooptic properties have been made. The measured electrooptic FOM for DAST of 1700 pm/V at 820 nm compares favorably with other organic and inorganic materials. These studies support the tremendous potential of organic salt crystals for providing highly nonlinear, thermally stable organic materials for optical signal processing, communications and interconnect applications.

Acknowledgment. The research described in this paper was performed in part by the Jet Propulsion Laboratory, California Institute of Technology as part of its Center for Space Microelectronics Technology and was supported by the Advanced Research Project Agency and the Ballistic Missile Defense Organization, Innovative Science and Technology Office through an agreement with the National Aeronautics and Space Administration (NASA). C.P.Y. wishes to acknowledge his wife Pamela for permission to work on this paper over the weekend and AFOSR contract F49620-91-C-0075. The authors thank their colleagues: G. Bourhill, E. Boden, O. Duchenaux, D. Fobare, S. Gilmour, P. Groves, B. Lawrence,

(75) Cook, W. R.; Jaffe, H. In *Electro-optic Coefficients;* Hellwege, K.-H., Ed.; Landolt-Bornstein, New Series Vol. 11; Springer-Verlag: Heidelberg, 1979; pp 552–651.
(76) Lipscomb, G. F.; Garito, A. F.; Narang, R. S. *J. Chem. Phys.* **1981**, *75*, 1509–1516.
(77) Knöpfle, G.; Bossard, C.; Schlesser, R.; Günter, P. *IEEE J. Quantum. Electron.*, in press.
(78) Bosshard, C.; Sutter, K.; Schlesser, R.; Günter, P. *J. Opt. Am. B* **1993**, *10*, 867.
(79) Thackara, J. Ph.D. Thesis, Stanford University, 1992.
(80) Xhang, X. C.; Ma, X. F.; Gin, Y.; Lu, T. M.; Boden, E. P.; Phelps, P. D.; Stewart, K. R.; Yakymyshyn, C. *Appl. Phys. Lett.* **1992**, *61*, 3080.

W. Lotshaw, K. J. Perry, P. Phelps, E. T. Sleva, K. R. Stewart, and B. Tiemann for technical assistance and many helpful discussions. In particular, we thank Lawrence Henling, Richard Marsh, and William Schaefer for performing the X-ray determinations in this paper. S.R.M. and J.W.P. thank Prof. P. Günter for providing his group's manuscript prior to publication. S.R.M. and J.W.P. also thank Debbie Chester for instantaneous secretarial help.

Supplementary Material Available: Representative syntheses of stilbazolium salts, ^{1}H NMR and elemental analytical data for salts of 1[1], 1[2], 2[1], 2[2], 3, 6, 7, 8, and 9, experimental details of data collection, ORTEP drawings of the cations 1[1]-$CH_3C_6H_4SO_3$, 2[1]$CH_3C_6H_4SO_3$, 8Cl$(H_2O)_4$, and 2[1]Cl$(H_2O)_4$ with atom numbering, final parameters of all the atoms and complete distances and angles (38 pages); observed and calculated structures factors (32 pages). See any current masthead page for ordering information.